# Bone fracture healing under Ilizarov fixator: influence of fixator configuration, fracture geometry and loading

Ganesharajah Ganadhiepan[1], Saeed Miramini[1], Minoo Patel[2], Priyan Mendis[1], Lihai Zhang[1]

[1] Department of Infrastructure Engineering, The University of Melbourne, Victoria 3010, Australia.

[2] Epworth Hospital Richmond, Victoria 3121, Australia.

**Running title:** Bone fracture healing under Ilizarov fixator

**Corresponding author:**

Associate Professor Lihai Zhang

Department of Infrastructure Engineering, The University of Melbourne,

Victoria 3010,

Australia.

Phone: +61-3-87447179

Fax: +61-3-83444616

E-mail: lihzhang@unimelb.edu.au

This is the author manuscript accepted for publication and has undergone full peer review but has not been through the copyediting, typesetting, pagination and proofreading process, which may lead to differences between this version and the Version of Record. Please cite this article as doi: 10.1002/cnm.3199

## Abstract

**[1]** This study aims to enhance the understanding of the relationship between Ilizarov fixator configuration and its effects on bone fracture healing. Using Taylor spatial frame (TSF) as an example, the roles of critical parameters (i.e. TSF ring diameter, wire pretension, fracture gap size and axial load) that govern fracture healing during the early stages were investigated by using computational modelling in conjunction with mechanical testing involving an advanced 3D optical measurement system. The computational model was first validated using the mechanical test results and then used to simulate mesenchymal stem cell (MSC) differentiations within different regions of the fracture site under various combinations of TSF ring diameter, wire pretension, fracture gap size and axial load values. Predicted spatially dependent MSC differentiation patterns and the influence of each parameter on differentiations were compared with *in vivo* results and good agreement was seen between the two. Gap size was identified as the most influential parameter in MSC differentiation and the influence of axial loading and TSF configuration (i.e. ring diameter and wire pretension) on cell differentiation was seen to be gap size dependent. Most changes in cell differentiation were predicted in the external callus (periosteal) which is the crucial region of the callus in the early stages. However, for small gap sizes (e.g. 1 mm) significant changes were predicted in the endosteal callus as well. The study exhibits the potential of computational models in assessing the performance of Ilizarov fixators as well as assisting surgeons in patient specific clinical treatment planning.



**Keywords**: Mechanoregulation, Taylor spatial frame, mesenchymal stem cell, mechanical test, 3D optical measurement system.

## 1 Introduction

**[2]** Minimally invasive surgical procedures to treat bone fractures have gained interest during recent decades [1-3]. This has led to the evolution of different external fixator devices with variety of capabilities. The main advantage of external fixators over the alternatives is their adjustability of configurations according to how healing progresses and thereby enabling better microenvironments to be achieved at the fracture site throughout the healing process [3].

**[3]** An important achievement in the realm of external bone fixator devices is the advent of Ilizarov circular fixator (ICF), which minimises the invasion into the bones by using very fine pretensioned wires (e.g. diameters 1.5 – 1.8 mm ) [4,5]. ICF is very effective in treating complex and unstable bone fractures [6] and a variety of other bone defects such as non-union, deformity, osteomyelitis and leg length discrepancy [7]. One of the key advantages of ICF is that it allows patient specific fixator configurations to be deployed by varying the assembly of the fixator components such as modular rings, threaded rods and pretension wires.

**[4]** Taylor spatial frame (TSF) is an advanced variant of ICF, which uses a hexapod system with six adjustable length telescopic struts at the fracture site (Fig.1). The hexapod system is advantageous over the conventional 'ring and threaded rod' system in ICF, as it allows the fracture site to be adjusted three dimensionally with six degrees of freedom, which enables TSF to correct almost any multiplanar deformity easily and accurately [8,9]. Thus, it makes TSF one of the most versatile external bone fixator devices. Most importantly, due to its feature of computer aided fixator adjustment, TSF is regarded as more reliable than the conventional ICF [10].

**[5]** It is known that mechanical stimulation highly influences the mechanical microenvironment at the fracture site and affect the healing process [11,12]. Therefore, good understanding of the mechanical performance of fixators is of great importance when treating

bone fractures. The mechanical stiffness of a fixator affects the interfragmentary movement (IFM) at the fracture site which is of critical importance; therefore, IFM should be controlled optimally to achieve timely and successful healing [13].

**[6]** Numerous experimental studies have investigated the influence of ICF frame elements and configurations on the biomechanical properties of the conventional ICF [4,14-16]. However, there is only limited amount of data available on the biomechanical properties of TSF under different configurations[8]. Henderson et al.[9] investigated the influence of ring-strut angle on the fixator stability using an isolated TSF hexapod. Khurana et al.[17] compared the effect of wires and half pins using a single ring experimental setup. However, these studies mainly focused on isolated behaviour of different parts of TSF. A few other studies investigated the mechanical behaviour of different TSF constructs by using tubes to represent bones[8,18]. However, the influence of the stiffness characteristics of the frame constructs (TSF) on the fracture site movements (i.e. IFM) has not been fully investigated yet. This is one of the current areas of interest in orthopaedic research [8,19].

**[7]** Computational methods are becoming increasingly popular in orthopaedic research [20-24]. Several mechano-regulatory algorithms for predicting mechanobiological processes of fracture healing have been proposed so far [24,25]. Based on these algorithms, numerous computational models were developed to study the influence of different fixator devices on fracture healing [20,22,26]. However, computational studies on TSF or its influence on fracture healing are very limited and it is still not clear how TSF configuration alters the fracture microenvironment and affect the healing process.

**[8]** By developing computational models in conjunction with mechanical testing (Fig. 2), the present study aims to investigate the influence of TSF configuration (i.e. ring diameter and wire pretension) on the mechanical microenvironment of the fracture site. In addition, the

effects of the axial loading and fracture gap size on the fracture microenvironment are also investigated. The current study mainly focuses on the early stage of fracture callus (i.e. post inflammatory phase callus consisting of granulation tissue) as it has been shown that the early stage fracture site is very critical and decisive of the cell fate which could affect the entire healing process [27,28].

## 2 Materials and Methods

**[9]** Mechanical tests were carried out on surrogate bone specimens with transverse fractures stabilized by a two ring TSF (Fig. 1a). The details of the experimental setup are shown in Fig. 3. The specimens were axially loaded using INSTRON universal testing machine and the interfragmentary movements (IFM) were measured using a 3D optical measurement system (ARAMIS). The IFM measurements were then used to validate the numerical predictions made using a computational model developed in this study (Fig.4). After model validation, the computational model was used to predict the mesenchymal stem cell (MSC) differentiation within the early callus under different combinations of gap size, axial load, ring diameter and wire pretension.

### 2.1 Mechanical Testing

**[10]** The surrogate adult human tibiae manufactured by SYNBONE AG (Malans, Switzerland) was used in the mechanical testing. The bone is made of specially formulated polyurethane foam that has the mechanical properties similar to those of adult human tibiae [21,29]. It comprises of outer cortical bone and inner cancellous bone and imitate the anatomical structure of a real bone very closely. The average compressive Young's modulus and Poisson's ratio of the surrogate bone are 1500 MPa and 0.25 respectively [21] and the surrogate bone fractures were stabilized using TSFs, manufactured by Smith & Nephew PLC (Memphis, Tennessee, USA).

**[11]** The coordinate system shown in Fig. 1 (and explained under section 2.5) was adopted in this study. Each TSF construct used in the mechanical test (Fig. 3) consisted of (i) two identical aluminium rings (one for the proximal fragment and another for the distal fragment); (ii) four 1.8 mm diameter stainless steel pretension wires (two mutually perpendicular wires per ring; one parallel to X and another parallel to Y direction), and (iii) six FAST FX struts (Smith & Nephew) per assembly. The rings and FAST FX struts were assembled to have a ring-strut angle of 65˚ (as shown in Fig. 1b) and the bone specimens were centred to the rings. The wires were affixed to a drill driver (Milwaukee, Wisconsin, USA) and their bayonet ends were used to directly drill through the bones and secured in position at both ends of the rings with slotted wire fixation bolts. Once the TSF was affixed to the bones, a 20 mm fracture gap was created at mid height of the tibia. The reason for choosing a relatively larger gap size was to prevent bone fragment apposition during loading.

**[12]** In the next step, the wires were pretensioned by keeping one end of the wire tightly fixed to the ring using slotted wire fixation bolts and nuts and stretching the other end using a dynamometric wire tensioner (Smith & Nephew). This device provides graduations of the standard range of clinical wire pretension levels in kilograms (i.e. 50 – 130 kg) which was used to measure the pretension level in the wires as they were stretched. Once the desired pretension was achieved, the wire tensioner was locked in position and the wire was secured to the ring tightly at the stretching end using slotted wire fixation bolts and nuts.

**[13]** Two different TSF constructs, one with 130 mm ring diameter and another with 155 mm ring diameter were used in the mechanical testing. It should be noted that these diameters refer to the internal diameter of the rings. In both cases, wire pretension of 883 N (90 kg) was applied to all wires. The distal bone ends of the assembled TSF constructs were fixed to a lathe chuck and the assembly was loaded at the intercondylar eminence of the tibia in the -Z

direction using the universal testing machine (INSTRON 5569A, Massachusetts, USA). This test setup resembles the physiological load application (e.g. standing) on tibia from knee and ankle joints [21,30].

**[14]** With the help of the cross hairs of ARAMIS, the specimens were placed in the INSTRON machine each time carefully so that the fragments are vertical and properly aligned. This was done to ensure that the compressive load is applied axially (-Z direction) and to minimize the lateral movements of the fragments during axial loading. To simulate a partial weight bearing condition after surgery, an axial compressive load of 150 N (i.e. around 20 % of the body weight) was ramped over 0.5 s [29] using the INSTRON machine. Each test was repeated five times and the IFMs were recorded using ARAMIS 3D optical measuring system at 25 N intervals.

2.1.1 IFM measurement using ARAMIS 3D optical measuring system

**[15]** The purpose of this mechanical test is to measure the fracture site movements at number of points along the fracture ends rather than at just one point (e.g. mid-point) using the ARAMIS 3D optical measuring system (GOM, Braunschweig, Germany); which, allows full field measurements at multiple points to be taken simultaneously. ARAMIS provides very accurate non-contact measurements, eliminating the sources of measurement errors that are present in contact measurements. It can measure deformations as small as 0.0002 mm with a strain accuracy of 0.01 %; thus, making the effect of measurement errors insignificant for the range of displacements measured in this experiment (Fig. 4).

**[16]** To capture the displacements using ARAMIS, a stochastic speckle pattern consisting of black dots on white background was created using spray paints around the fracture gap of the tibia (Fig.3) as per the specifications of the GOM [31]. ARAMIS creates facets (small

rectangular areas) from this speckle pattern and uses them to determine the displacements based on the relative movements of the facets between subsequent images captured.

**[17]** In this study, two cameras (50 mm focal length lenses) of the ARAMIS system, set up according to the specifications of GOM [31] were used to capture the images. The facets were of 19 x 19 pixel (15 x 15 pixels with 2 pixel overlapping) which is the recommended facet size of ARAMIS for normal deformation measurements [31]. Before each test, to ensure that the speckle pattern is adequate, an image covering the fracture gap and the surrounding areas with speckle pattern was captured and processed using the ARAMIS control machine (Fig. 3) to see if ARAMIS could detect the fragment ends and the surrounding areas which is the area of interest. Mechanical test and displacement measurements were carried out only after ensuring this.

**[18]** Full field (i.e. X, Y, Z) displacements of multiple points along the proximal end of the fracture gap and the corresponding points (lying vertically below) in the distal end of the fracture gap were measured and the relative movements between the proximal points and the corresponding distal points were calculated as IFM in each direction. In each test, the first image was captured when the axial load was zero and then images were captured at every 25 N intervals up to 150 N.

## 2.2 Computational modelling

**[19]** To study the influence of ring diameter, wire pretension, gap size and axial load on the early fracture microenvironment, a 3D computational model of the fractured tibia with TSF was developed (Fig. 1b). The 3D geometry of the tibia was reconstructed from CT scan images of the surrogate tibia, which enabled the tibial geometry to be reconstructed with its the inner open volumes. The geometry was then imported to the commercial CAD software SOLIDWORKS (Dassault Systèmes, Massachusetts, USA) where the geometric operations

were carried out. The finalised geometry of the fractured tibia was then imported to the commercial finite element software package COMSOL MULTIPHYSICS (COMSOL AB, Stockholm, Sweden) where the geometry of the TSF was developed around the tibia. Subsequently meshing and numerical analysis were conducted using COMSOL MULTIPHYSICS.

**[20]** First, the computational model was validated using the axial IFMs measured in the mechanical test. The purpose of this validation process is to ensure that the computational model could be implemented to simulate IFMs (mechanical stimulus for cell differentiation within the callus) under different combinations of the parameters studied (e.g. wire pretension, axial load etc.). As shown in Fig. 2, to simulate the mechanical test, the model was created with a gap at mid height of the tibia and the material properties of SYNBONE surrogate tibia were assigned to the bone fragments. The TSF components (i.e. aluminium rings, stainless steel FAST FX struts and stainless-steel pretension wires) were modelled as linear elastic materials and the axial loading was applied as a point load to represent the narrow loading region in the mechanical test (Fig. 2). The IFM predictions were then compared with the mechanical test results. After validation, our previously developed poroelastic callus model [21,22,29] was imported into the model and added around the fracture gap as shown in Fig.2 where the bone-callus interface was connected using continuous solid to solid connections. The properties of the materials used in this study are given in Table 1.

## 2.3 Governing equations

**[21]** Based on the theory of porous media, the mechanical behaviour of the early stage fracture callus could be explained as given below [22,32]. The stress tensor $\boldsymbol{\sigma}$ of the callus could be expressed as

$$\boldsymbol{\sigma} = -p\mathbf{I} + \boldsymbol{\sigma}^{\mathbf{e}} \quad (1)$$

where, $p$ is the incremental interstitial fluid pressure, $\mathbf{I}$ an identity matrix and $\boldsymbol{\sigma}^{\mathbf{e}}$ the elastic stress of solid matrix [22]. Neglecting the body forces and assuming that the tissue is under quasi static condition, the momentum equation could be expressed as [22] :

$$\nabla.\boldsymbol{\sigma} = -\nabla p + \nabla.\boldsymbol{\sigma}^{\mathbf{e}} = \mathbf{0} \quad (2)$$

where, $\nabla p$ is the gradient of $p$, $\nabla.\boldsymbol{\sigma}$ and $\nabla.\boldsymbol{\sigma}^{\mathbf{e}}$ are the divergences of $\boldsymbol{\sigma}$ and $\boldsymbol{\sigma}^{\mathbf{e}}$, respectively.

[16] The continuity of solid and fluid phases could be expressed by the following divergence equation:

$$\nabla.(\mathbf{v}^{\mathbf{s}} - \mathbf{k}\nabla p) = \mathbf{0} \quad (3)$$

where, $\mathbf{v}^{\mathbf{s}}$ is the velocity of the solid phase and $\mathbf{k}$ is the tissue permeability tensor.

2.4 Mechano-regulation

**[22]** Several mechano-regulatory theories for fracture healing have been proposed so far [25,33-36]. These theories either use a combination of mechanical parameters such as principal strain and hydrostatic stress [33], strain and hydrostatic pressure [34], deviatoric strain and fluid velocity[23,25] or single mechanical parameter such as interfragmentary strain [35] or deviatoric strain [36] to simulate the mechano-regulation at fracture site. Isaksson et al. [24] compared several of these mechano-regulatory theories with *in-vivo* sheep experimental data and concluded that the algorithm for poro-elastic formulations based on deviatoric strain and fluid velocity by Prendergast et al. [23,25,37] was reasonably accurate, more versatile and shows better agreement with the experimental observations than the alternatives. Therefore, we incorporated the theory of Prendergast et al. [23,25,37] in the present study along with the material properties (Table 1) used in their models.

**[23]** The mechano-regulatory theory of Prendergast et al [25,37] suggests that the differentiation of mesenchymal stem cells (MSC) into osteoblast, chondrocytes or fibroblasts depends on the stimulation index *'S'* ($S = \gamma/a + v/b$ ; where, $\gamma$ is the octahedral shear strain of solid phase, $v$ is the interstitial fluid flow, $a$ = 0.0375 and $b$ = 3 μm $s^{-1}$) [23,37]. During the early stage fracture healing, small magnitudes of $S$ ( < 1) would lead to osteoblast differentiation, $S$ in the range of $1 < S < 3$ would lead to chondrocyte differentiation, while large magnitudes of $S$ ( > 3) would lead to fibroblast differentiation [37].

2.5 Boundary conditions and loading protocol

**[24]** In this study, the early callus was assumed to be filled with MSC, and its external boundaries were assumed to be impermeable to fluid flow [24]. As shown in Fig. 1, a right-handed Cartesian coordinate system was used in the model with positive X pointing the anterior direction; positive Y pointing the medial direction; and positive Z pointing proximal direction. Wire pretensions were applied as initial stress (initial condition at t = 0) to the wire elements along their axial direction (i.e. either X or Y direction depending on the orientation of the wires). The bottom end of the distal fragment was fixed. The axial compression was then applied over a period of 0.5 seconds at the top of the proximal end (in the -Z direction) as depicted in Fig. 1b.

**[25]** In real circumstances, around 60 % of the knee load is taken by the medial condyle and 40 % is taken by the lateral condyle [38]. Therefore, the distribution of the load on the tibial plateau is generally nonuniform across the surface [38]. For simplification, the axial load could be as uniformly distributed loading applied on the tibial plateau [39], and this simplification would have little effect on the mechanical microenvironment of the bone cells. During the mechanical test, the pretension wires drilled through the bones had a very firm grip on the bones. Therefore, the wire-bone interface was modelled using rigid connections as in the

study of Nielsen et al. [40] and the simulation results fitted the experimental data reasonably well (Section 3.1).

### 2.6 Geometric non-linearity of pretension wires

**[26]** The relationship between the transverse load and the corresponding deflection of the pretension wires is generally non-linear [41] due to the stress stiffening effect of the wires which tends to increase the resistance to deflection as the transverse load increases [2]. Therefore, the geometric non-linearity of the wires was considered in the analysis.

### 2.7 Numerical solutions

**[27]** As shown in Fig. 1b, the entire fracture geometry was meshed using second order solid tetrahedral elements. A mesh convergence analysis was conducted to determine the optimum mesh size for the model and the numerical model was solved using the time dependent solver with absolute tolerances of $10^{-1}$ Pa and $10^{-4}$ m for pore pressure and displacement, respectively. These tolerance values were chosen based on the degree of accuracy required for the solution and computational efficiency. Based on our previous studies [22,29], the dependent variables, i.e. displacement and pore pressure were calculated to $10^{-4}$ m (or 0.1 mm) and $10^{-1}$ Pa (or 0.1 Pa) accuracies. The mesh sizes were chosen such that the differences between subsequent solutions in the convergence analysis were less than 2 %. As pore pressure and fluid velocity are rapidly changing variables within the callus, the convergence analysis resulted in finer mesh for the callus than the other elements in the model. The entire geometry was meshed with 216496 and 207595 tetrahedral elements for 155 mm and 130 mm ring TSFs respectively.

### 2.8 Parametric studies

**[28]** Using the developed computational model, a series of parametric studies were conducted to investigate the influence of different TSF configurations, fracture gap sizes and loading conditions on cell differentiations within the callus during the early stage of healing. Two different ring diameters (i.e. 130 mm and 155 mm) and three different wire pretensions (i.e. 491 N (50 kg), 883 N (90 kg) and 1275 N (130 kg)), gap sizes (i.e. 1 mm, 3 mm and 5 mm) and axial loads (i.e. 100 N, 150 N and 200 N) were considered in this study as shown in Table 2. The cell differentiations within different regions of the fracture callus, namely, periosteal callus, intercortical callus and endosteal callus (Fig. 5b) were numerically predicted under each of the cases (Table 2).

## 3 Results

### 3.1 Model validation

**[29]** The mechanical test results showed that the IFMs were predominantly vertical (Z direction) and both vertical and lateral components (X ,Y directions) of IFMs increased with axial load. However, the largest lateral IFMs (X or Y direction) were observed to be 0.077 mm and 0.101 mm for TSF with 130 mm and 155 mm diameter rings respectively at 150 N axial load. The corresponding model predicted IFMs were 0.073 mm and 0.097 mm respectively which are close enough to the mechanical test results (5 % and 4 % respectively). Since the lateral components (X or Y) of the IFMs were negligible compared to the vertical components (less than 2.5 % of the Z components for both rings), the lateral and rotational components were ignored from further analysis. Therefore, IFM would refer to the axial IFM (Z direction) hereinafter.

**[30]** To obtain a more representative value of the IFM, the mean values of IFMs were calculated from three points along the proximal end and the corresponding points in the distal ends. Fig. 4 compares the mean axial IFM components calculated from the mechanical test

with those predicted numerically. The non-linear relationship between axial load and IFM can be seen in Fig. 4 which is due to stress stiffening effect of the pretensioned wires [41]. This nonlinearity is geometric as reported in many studies [41-43] and depends on the level of transverse movements of the wire. This explains the difference in the nonlinearities under different ring sizes. It was observed that the numerical predictions were either within the experimental error range or very close to the mean IFM values (maximum of 7 % deviation) for the entire range of loading considered. Therefore, the developed computational model could reproduce the mechanical experiment reasonably well.

### 3.2 Parametric studies

#### 3.2.1 Spatially dependent MSC differentiation pattern

**[31]** After validation, the model was used to investigate the effects of fracture gap size, axial load, TSF ring diameter and wire pre-tension on MSC differentiations during the early stage healing. Fig. 5 shows cell differentiations within the fracture callus, stabilized with TSF (ring diameter = 155 mm, wire pre-tension = 883 N (90 kg) and axial load = 150 N) under different gap sizes (i.e. 1 mm, 3 mm and 5 mm). It can be seen that, MSC differentiation in the fracture callus is spatially dependent with osteoblast differentiation in both proximal and distal ends of the external callus (i.e. periosteal callus) far from the fracture gap, chondrocyte differentiation in the external callus and fibroblast differentiation within the internal callus (i.e. intercortical and endosteal callus).

**[32]** Histological observations of early stage bone fracture healing [44-46] have shown that (i) bone forming from intramembranous ossification (i.e. directly from osteoblasts) takes place farther away from the fracture site in the external callus adjacent to periosteum where the interfragmentary movements cause very little strain; (ii) formation of cartilaginous tissue from chondrocyte differentiation takes place in the external callus adjacent to the fracture

line; and, (iii) fibrous connective tissue forms within the fracture gap and between the cartilaginous zones where the tissue strains are high. It can be seen that, the predicted differentiation patterns in Fig. 5 agree reasonably well with patterns observed histologically [44-46]. Furthermore, as shown in Fig. 5, the model predicts that the internal and external callus regions are in different mechanical microenvironments. The internal callus is affected more than the external callus as a result of IFM which concurs with other studies in the literature [12,23]. Figures 6-9 presents the influence of each parameter (i.e. gap size, axial load, wire pretension and ring diameter) on the cell contents within different regions of the callus (i.e. periosteal, intercortical and endosteal). But, the results of callus regions where there were no significant changes (all changes < 5%) are not presented.

3.2.2 Gap size

**[33]** Figure 6 shows the change of fibroblast, chondrocyte and osteoblast contents relative to the control case G3 (i.e. gap size = 3mm (Table 2)) under different gap sizes (i.e. 1 mm and 5 mm). The results show that cell differentiation is very sensitive to gap size. Decreasing the gap size from 3 mm to 1 mm increased the osteoblast content by around 120 % but decreased the chondrocyte and fibroblast contents by around 70 % and 90 %, respectively in the periosteal callus. On the other hand, increasing the gap size from 3 mm to 5 mm, increased the fibroblast content in the periosteal callus by around 80 % but decreased the osteoblast content by around 55 %. In the intercortical callus, the changes were relatively small (< 4 %) and the cells were mostly fibroblasts. However, in the endosteal callus, chondrocyte content increased (by 35 %) and the fibroblast content decreased (by 35 %) as the gap size decreased from 3 mm to 1 mm. But, no noticeable changes were seen as the gap size increased.

3.2.3 Axial load

**[34]** Figure 7 shows the changes in cell contents within different zones of the callus under different axial loads (i.e. 100N and 200N) relative to control case (i.e. axial load = 150N (Table 2)). It indicates that the influence of axial load on cell differentiation is location and gap size dependent. For example, under a small gap size (i.e. 1mm), the change in the magnitude of axial load had little influence on osteoblast content; however, under mid and large gap sizes (i.e. 3mm and 5mm), obvious increase (i.e. up to 45%) was seen in the periosteal callus when reducing axial load from 150N to 100N. In the endosteal and cortical callus no noticeable changes were seen in the osteoblast content.

**[35]** Differentiation of chondrocytes in the periosteal zone, increased with the axial load for small and medium sized gaps (i.e. 1 mm and 3 mm); however, under a large gap size (i.e. 5 mm), increase in axial load predicted decrease in chondrocyte content. The fibroblast content in the periosteal callus generally increased with the axial load and the increase was more significant under relatively small gap sizes (e.g. 1 mm) as shown in Fig. 7. No noticeable changes in the chondrocyte or fibroblast contents were predicted in the intercortical or endosteal callus due to changes in axial load magnitude for mid and large gap sizes (i.e. 3 and 5 mm). However, for 1 mm gap, endosteal callus showed increase of chondrocytes (up to 80 %) and decrease of fibroblasts (50 %) as the load reduced to 100 N; but, decrease of chondrocytes (up to 60 %) and increase of fibroblasts (35 %) were noticed as the load increased to 200 N.

3.2.4 TSF ring diameter and wire pretension

**[36]** Figure 8 shows the changes in cell contents within different callus regions under 130 mm diameter ring relative to control case (i.e. ring diameter = 155mm (Table 2)) for different gap sizes. The results show that decreasing the ring diameter from 155 mm to 130 mm affects osteoblast content significantly (around 20 % increase); but, only in the periosteal callus for

large gap sizes (e.g. 5mm). The increase in TSF mechanical stiffness resulting from the reduction of the ring diameter from 155 mm to 130 mm was insufficient to affect the fibroblast or chondrocyte contents significantly except in the endosteal callus for small gap sizes (e.g. 1 mm) where chondrocytes increased and fibroblasts decreased by 20 % and 15 % respectively.

**[37]** Figure 9 shows the effects of different wire pretensions on cell contents within different regions of the callus relative to control case (i.e. 883N or 90 kg (Table 2)). The changes in wire pretension significantly changed the osteoblast content (around 10 %) only in the periosteal callus under a large gap size (i.e. 5 mm). The fibroblast contents did not change significantly by changing the wire pretensions and the chondrocyte content was also not predicted to change significantly, except in the endosteal callus for a small gap size (i.e. 1 mm) where 10 % increase was observed as the wire pretension increased to 1275 N.

## 4 Discussion

**[38]** Differing from previous studies in literature which mainly focus on the mechanical behaviour of Ilizarov fixator (TSF), the current study provides a mechanobiological perspective to its performance. A single fully coupled 3D computational model of Ilizarov fixator (TSF) including poroelastic soft tissues of bone is presented in this study. This enables mechanobiological assessment of the effects of fixator configuration and patient specific geometric and load conditions on the biomechanical microenvironment of the fracture site.

**[39]** Since the axial stiffness of TSF is dependent upon the IFM itself (due to stress stiffening of pretensioned wires), important parameters that affect IFM such as gap size and axial load were also considered in this study along with TSF ring diameter and wire pretension. The

present study closely mimics the realistic bone fracture conditions stabilized by TSF and a range of clinically relevant values were chosen for the parametric studies. *i.e.* (i) Axial loading ranging from 100 N to 200 N, which represents the allowable weight bearing after surgery [21]; (ii) Common wire pretensions ranging from 491 N (50 kg) to 1275 N (130 kg) [4]; and (iii) TSF ring diameters of 130mm and 155mm (Smith & Nephew).

**[40]** It should be noted that ring-strut angle plays an important role in the stability of TSF. An experimental study [9] showed that TSFs would reach instability as the ring-strut angle reduces and recommended to avoid ring-strut angles less than 30°. The study also showed that TSFs are generally stable under compression for ring-strut angles in the range of 30-70° with larger angles leading to lower stresses in the struts which could be explained using simple truss mechanics. Therefore, we adopted a ring-strut angle of 65° in this study (Fig. 1).

**[41]** In this study, the effects of each parameter (i.e. gap size, axial load, ring diameter and wire pretension) and their interactions on the fracture environment were studied numerically using the computational model based on predicted cell differentiations (mechanobiological performance). The purpose of the mechanical test was to only validate the computational model and not to study the mechanical performance of the fixator under different parametric values as many studies in literature [2,4,17] have already done this. However, we carried out a two-way ANOVA test on the mechanical results which revealed that both axial load and ring diameter have strong effects on the axial stiffness of the fixator ($p < 0.05$) with ring diameter having the strongest effect. However, their interaction did not appear to affect the axial stiffness significantly ($p = 0.06$).

**[42]** In the mechanical test, we ensured no bone apposition during loading by creating a large gap (i.e. 20 mm) in the tibia due to the fact that, if the fragments get into contact under loading, the load could pass directly through the contact surface, making the fixator

ineffective. In general, flexible fixations such as TSF are ideally expected to permit interfragmentary strains (IFS) around 10 – 30 % for the best healing outcomes [12,22,47]. IFSs above 30 % are considered high [12,48] and may have detrimental effects on healing. IFS due to loading depends on the flexibility of the fixator. An Ilizarov fixator that is too flexible (unstable) may result in large IFMs and even bone apposition under partial weight bearing [49-51] leading to very high IFSs which are detrimental to healing. Therefore, surgeons generally strive to achieve moderate IFS by limiting the IFM.

**[43]** Although the computational model developed in this study mainly focuses on the early stage cell differentiations within the callus, it provides very useful data for two reasons. Firstly, the early microenvironment is of prime importance as it is decisive of the cell fate and affect the healing pathway of the progenitor cells and subsequently the entire healing process [27,28]. Secondly, the fixator's role in the fracture stability is predominant in the early stage [1], when the fracture callus stiffness is too low with very soft tissues.

### 4.1 Predictive capacity of the model

**[44]** The predictive capacity of the developed computational model was assessed by comparing the IFMs predicted by the computational model with the IFMs measured experimentally using the ARAMIS 3D optical measuring system (Fig. 4). It was observed that the IFM predictions for 155 mm ring showed larger differences from the mechanical test compared to those of 130 mm ring. This could be possibly attributed to the relative movement of the wire in the bone-wire interface. As the wires deflect under transverse load, they tend to elongate and move relative to the bone. For 155 mm ring the effect would be more compared to that of 130 mm as the axial stiffness of 155 mm ring would be relatively low and the movements would be relatively big. Also, this effect would be more perceptible at relatively small loads, because the axial stiffness would be low at low loads. As the load

increases, the axial stiffness would increase due to stress stiffening effect and the incremental deflection of wires for a given load increment would get smaller. However, in the present model, the interface was modelled as rigidly connected to each other. Incorporating the relative movement in the computational model would have resulted in relatively more axial movements as reported in the study of Zamani and Oyadiji [43]. Nevertheless, it could be seen that the computational model can reproduce the experimental observations reasonably well as the numerical predictions were always either within the experimental error range or very close to the mean values (maximum of 7 % deviation).

**[45]** In addition, the model predicted cell differentiations were consistent with, *in vivo* observations [12,44-46] and predictions of well established computational models [23,24]. For example, the cell differentiation patterns predicted in this study (Fig. 5) concur with patterns observed in histological studies [44-46] and those predicted by the computational models of Lacroix and Prendergast [23] and Isaksson et al. [24]. In addition, the model predicted that the cell differentiations within the fracture gap is affected very much by the IFM; but, the effect of IFM gradually diminishes with the increase of distance from the fracture gap which is in line with other studies [23].

4.2 Parametric study and comparison with *in vivo* studies

**[46]** In studying human orthopaedic conditions, rat, mouse and rabbit models are the most commonly used in laboratories [52]. However, due to the size of these animals, their applicability is limited to basic orthopaedics and acceptable only in the early stages [52]. To study more complex issues (e.g. fracture fixations) larger animals with limbs and skeletal segments of sufficient sizes such as non-human primates, sheep, goats, dogs and pigs [52] are required. Among these, sheep is found to be (i) easy to handle; (ii) more feasible in terms of economy, emotions and ethics and (iii) similar to humans in terms of body weight [52]. A lot of

studies using external fixations have been carried out on sheep models in the past [12,53,54].The present study compares the model predictions with some of the relevant sheep experiment results in the literature.

**[47]** The model predicted that most of the changes resulting from parametric changes were within the periosteal region of the callus and the changes in the internal callus (intercortical and endosteal callus) were insignificant in most cases. This is because the internal callus would be highly affected (S >> 3) by IFM in the early stages of the healing and varying the external parameters within the physiological range would not be enough to turn the mechanical microenvironment favourable (S<=3). Only reducing the fracture gap to very small sizes (e.g. 1 mm) could stabilize the environment and make it more favourable for healing as observed in sheep experiments[12,53]. The present model was able demonstrate this as the internal callus was predicted to be favourable and responsive to other parameters only for 1 mm gap size (Fig 6-9).

**[48]** The changes in external callus (periosteal) are thought to be very crucial in the early stages as external callus plays the role of surrounding the fracture site and stabilizing it in the early stages so that the fracture site movements can be limited [36,44,45]. This would gradually turn the fracture site microenvironment favourable for healing (S<=3). Therefore, we focus mainly on the changes within this region of the callus.

**[49]** Among the four parameters explored in this study (i.e. gap size, axial load, ring diameter and wire pretension), gap size is the most critical parameter affecting the cell differentiations within the callus. As shown in Fig. 6, relatively smaller gap sizes (e.g. 1 mm) result in larger osteoblast differentiation within the periosteal callus, which is indicative of osteogenic pathway and faster bridging of the fragments. In contrast, larger gap sizes (e.g. 5 mm) lead to the increase of fibroblast content which is indicative of delayed healing. These observations

503 are consistent with the sheep experiment of Claes et al. [12] which investigated the roles of gap
504 size and fracture stability on fracture healing and indicated delayed healing with the increase
505 of gap size from 1 to 6 mm. This observation could be attributed to the increase of
506 interfragmentary strain (IFS) with gap size (when all other parameters are kept unchanged)
507 [12,23]. Smaller IFSs (under small gap sizes) result in more stable mechanical
508 microenvironments (S<1) which is conductive to osteoblast differentiation, whereas
509 relatively unstable microenvironments (S>3) resulting from larger IFS (under large gap sizes)
510 are conductive to fibroblast differentiation.

511 **[50]** The present study suggests that the chondrocyte content is high in the periosteal region
512 of mid-sized (e.g. 3 mm) fractures (up to 70 % more than other gap sizes) which is indicative
513 of greater cartilage tissue formation (Fig. 6). This prediction is also comparable with the
514 results of the sheep experiment [12] which reported that a 2 mm gap size induced more
515 cartilage formation (up to 60 %) than those of 1 mm or 6 mm gap sizes [12]. This is because
516 mid-sized gaps (i.e. 3 mm) result in moderate IFSs which gives rise to mid-range S values
517 (i.e. 1<S<3) within the callus which is conductive to chondrocyte differentiation and
518 subsequently cartilage formation.

519 **[51]** Physiologically relevant loading imposed on the fractured bone after surgery is another
520 important factor that influences the healing outcomes. The results in Fig. 7 show that the
521 increase of axial load (from 150 N to 200 N) could increase the fibroblast content (up to 60
522 %) but decrease the osteoblast content (up to 25 %) in the periosteal callus. However,
523 chondrocyte content could increase with the axial load only for small (i.e. 1 mm) and mid-
524 sized (i.e. 3 mm) gaps (up to 45 % and 5 % respectively). For large gap sizes (i.e. 5 mm)
525 chondrocyte content tends to decrease with the axial load (up to 15 %). This observation too
526 concurs with the sheep experiment results of Claes et al.[12] where IFS increase from 7 % 31 %

resulted in callus area increase of 19 % and 29 % for 1 mm and 2 mm gaps respectively; but a 37 % decrease for 6 mm gap. This is because fractures with relatively small and mid-sized gaps (i.e. 1-3 mm) are relatively stable. Therefore, moderate loading (100 – 200 N) would give rise to moderate stimulation (1<S<3), increasing the chondrocyte content. However, for relatively large gaps (i.e. 5 mm), where the fracture site is unstable, the same magnitude of load would result in larger IFS and hence higher S values (S>3), which could lead to increase in fibroblast differentiation. The implication of the model predictions is that the amount of weight bearing has to be carefully chosen considering the patient specific parameters such as gap size to prevent delayed healing or non-union.

**[52]** Within the range of values considered in this study, the stiffness changes due to change of TSF ring diameter or wire pretension appeared to be insufficient to make significant changes to the cell contents within the periosteal callus for small and moderate gap sizes (i.e. 1 – 3 mm). However, for a large gap size (i.e. 5 mm) significant changes were observed, especially with osteoblast content (Fig.8 and Fig. 9). The results suggest that, in the early stages of healing, for small or mid-sized fractures (i.e. 1-3 mm), controlling the loading (i.e. partial weight) could be more effective than striving to modify the stiffness of TSF by changing the wire pretension or ring diameter. However, for relatively large gap sizes (e.g. 5 mm) surgeons would also have the option of adjusting these parameters to a certain extent to control biomechanical microenvironment of the fracture site. But the most important of all is careful reduction of the fragments; because, it would decide the gap size which is the most influential parameter of all.

**[53]** In the internal callus (intercortical and endosteal), it could be seen from Fig. 6 that reducing the gap size to 1 mm from 3 mm could result in chondrocyte increase and fibroblast decrease (around 35 % each) in the endosteal region. Furthermore, Fig. 7-9 show that

significant changes occur in the endosteal callus in response to other parameters only for 1 mm gap size. In general, stabilizing the fracture site increases chondrocyte content and decreases fibroblast content within the endosteal zone for small gap sizes (e.g. 1 mm). For example, decreasing the axial load (from 150 N to 100 N) or decreasing the ring diameter (from 155 mm to 130 mm) or increasing the wire pretension (from 883 N to 1275 N) could increase the chondrocyte content up to 80 %, 20 % and 10 % and decrease the fibroblast content up to 50 %, 15 % and 5 % respectively. The histological observations of sheep osteotomy sites by Claes et al.[55] showed fracture bridging to take place via both periosteal and endosteal callus for all sheep with 1 mm osteotomy which was not observed for sheep with 2 mm or 6 mm osteotomies. In addition, increasing the gap size from 1 mm to 2 mm and increase of IFS from 7 % to 31 % in the 1 mm group was observed to considerably increase the fibrous connective tissue within the fracture site. These observations are in agreement with the model predictions of this study.

**[54]** A different sheep study by Yamaji et al. [53] with external ring fixators have indicated that even a larger IFS (35 %) in smaller fractures (2 mm) could result in relatively lesser connective tissues (around 50 %) within the callus than those with a smaller IFS (12 %) in larger fractures (6 mm). So, it appears that smaller fracture gap sizes could result in better mechanical microenvironments throughout the callus.

**[55]** Because of this, it is recommended that reduction of fragments need to be carried out carefully under flexible fixations such as TSF to improve fracture healing [12]. Generally, it is suggested that reductions should be made with small gap sizes as possible [12]. However, relatively large gap sizes (i.e. 5 mm or more) may sometimes become inevitable in clinical situations. Especially, where there is significant bone loss due to high energy fractures [56] or surgical removal of bone tumours [7].

**[56]** Therefore, to determine the most desirable environment within the fracture site, it is necessary to consider the patient specific parameters such as gap size and loading levels along with the fixator stiffness parameters. In this regard, models like the one presented in this study would be of assistance to surgeons in making patient specific treatment planning.

### 4.2 Limitations

**[57]** It is known that tibial bone is an anisotropic material, the mechanical properties of which depend on its microstructure and mineral composition [57]. Therefore, the mechanical response of human tibia in different directions would be different [57,58]. However, in this study, mechanical tests were carried out using surrogate tibia and the bone tissues were assumed to be isotropic to simplify the computational analysis.

**[58]** It should be mentioned that, to simplify the complex loading scenarios, only axial compressive load (representing knee joint loading as uniform compression) was considered and the growth of fracture callus and change of mechanical properties were ignored in this study. In addition, bio-regulatory effects (e.g. growth factors) were not considered in this study. Moreover, as the current study was focused on the early stage, only the initial response is predicted in this study. Most importantly, further experimental and clinical evidence is required to validate the model predictions.

## 5 Conclusions

**[59]** The outcomes of this study provide new insights (in a mechanobiological perspective) into the use of Ilizarov fixator (TSF) in treating bone fractures. The computational model developed in this study enables the selection of optimal parameters (i.e. fracture gap, TSF ring diameter, wire pretension and axial loading) during the early stage fracture healing. A summary of the main findings of this study are as follows:

- The developed model was able to predict the spatially dependent MSC differentiation patterns observed in histological studies. Also, the numerical predications from the parametric study concur well with *in vivo* observation which exhibits the potential of numerical modelling in assisting treatment planning.
- Gap size is the most important parameter that affects cell differentiations within the callus. Small gap sizes (e.g. 1 mm) could result in better healing microenvironments throughout the callus; whereas, mid (e.g. 3 mm) and large size (e.g. 5 mm) gaps tend to rely mostly on periosteal stabilization. Therefore, careful reduction of the fracture is of paramount importance.
- The influence of axial loading on cell differentiation is gap size dependent. The changes in cell differentiation due to axial load changes are mainly noticeable in the periosteal callus; but for small gap sizes (e.g. 1 mm) changes are noticeable throughout the callus.
- The change in TSF mechanical stiffness resulting from change of the ring diameter (i.e.155 mm to 130 mm) or wire pretension (491 N – 1275 N) could only change the cell contents in the periosteal callus significantly for large gap sizes (e.g. 5mm) and the changes are mainly noticeable in the osteoblast content. For smaller gap sizes (e.g. 1 mm) significant changes (up to 20 %) could be achieved within the internal callus as well.
- It is preferable to achieve gap sizes as small as possible. But, when larger gap size (e.g. 3 – 5 mm) are unavoidable, controlling the axial load (i.e. partial weight bearing) would be more effective than adjusting the TSF stiffness by changing the ring diameter or wire pretension in the early stages of healing.

**Conflict of Interest**

**[60]** No benefits in any form have been or will be received from a commercial party related directly or indirectly to the subject of this manuscript.


## Acknowledgements

**[61]** Authors would like to thank the support provided by The University of Melbourne.


## References


1. Goodship A, Watkins P, Rigby H, Kenwright J. The role of fixator frame stiffness in the control of fracture healing. An experimental study. *Journal of Biomechanics.* 1993;26(9):1027-1035.
2. Bronson DG, Samchukov ML, Birch JG, Browne RH, Ashman RB. Stability of external circular fixation: a multi-variable biomechanical analysis. *Clinical Biomechanics.* 1998;13(6):441-448.
3. Fragomen AT, Rozbruch SR. The mechanics of external fixation. *HSS Journal.* 2007;3(1):13-29.
4. Fleming B, Paley D, Kristiansen T, Pope M. A biomechanical analysis of the Ilizarov external fixator. *Clinical orthopaedics and related research.* 1989;241:95-105.
5. Antoci V, Voor MJ, Antoci V, Roberts CS. Effect of wire tension on stiffness of tensioned fine wires in external fixation: a mechanical study. *AMERICAN JOURNAL OF ORTHOPEDICS-BELLE MEAD-.* 2007;36(9):473.
6. Tucker HL, Kendra JC, Kinnebrew TE. Management of unstable open and closed tibial fractures using the Ilizarov method. *Clinical orthopaedics and related research.* 1992;280:125-135.
7. Erler K, Yildiz C, Baykal B, Atesalp AS, Ozdemir MT, Basbozkurt M. Reconstruction of defects following bone tumor resections by distraction osteogenesis. *Archives of orthopaedic and trauma surgery.* 2005;125(3):177-183.

8. Henderson DJ, Rushbrook JL, Harwood PJ, Stewart TD. What Are the Biomechanical Properties of the Taylor Spatial Frame™? *Clinical Orthopaedics and Related Research®.* 2017;475(5):1472-1482.

9. Henderson ER, Feldman DS, Lusk C, van Bosse HJ, Sala D, Kummer FJ. Conformational instability of the taylor spatial frame: a case report and biomechanical study. *Journal of Pediatric Orthopaedics.* 2008;28(4):471-477.

10. Keshet D, Eidelman M. Clinical utility of the Taylor spatial frame for limb deformities. *Orthopedic Research and Reviews.* 2016;55(unknown):51-61.

11. Goodship A, Kenwright J. The influence of induced micromovement upon the healing of experimental tibial fractures. *Bone & Joint Journal.* 1985;67(4):650-655.

12. Claes L, Augat P, Suger G, Wilke HJ. Influence of size and stability of the osteotomy gap on the success of fracture healing. *J Orthop Res.* 1997;15(4):577-584.

13. Duda GN, Eckert-Hübner K, Sokiranski R, Kreutner A, Miller R, Claes L. Analysis of inter-fragmentary movement as a function of musculoskeletal loading conditions in sheep. *Journal of biomechanics.* 1997;31(3):201-210.

14. Watson M, Mathias K, Maffulli N, Hukins D, Shepherd D. Finite element modelling of the Ilizarov external fixation system. *Proceedings of the Institution of Mechanical Engineers, Part H: Journal of Engineering in Medicine.* 2007;221(8):863-871.

15. Roberts CS, Antoci V, Voor MJ. The effect of transfixion wire crossing angle on the stiffness of fine wire external fixation: a biomechanical study. *Injury.* 2005;36(9):1107-1112.

16. Yilmaz E, Belhan O, Karakurt L, Arslan N, Serin E. Mechanical performance of hybrid Ilizarov external fixator in comparison with Ilizarov circular external fixator. *Clinical Biomechanics.* 2003;18(6):518-522.

17. Khurana A, Byrne C, Evans S, Tanaka H, Haraharan K. Comparison of transverse wires and half pins in Taylor Spatial Frame: a biomechanical study. *Journal of orthopaedic surgery and research.* 2010;5(1):23.

18. Tan B, Shanmugam R, Gunalan R, Chua Y, Hossain G, Saw A. A biomechanical comparison between Taylor's Spatial Frame and Ilizarov external fixator. *Malaysian orthopaedic journal.* 2014;8(2):35.

19. Kold S. CORR Insights®: What Are the Biomechanical Properties of the Taylor Spatial Frame™? *Clinical Orthopaedics and Related Research®.* 2017;475(5):1483-1485.

20. Byrne DP, Lacroix D, Prendergast PJ. Simulation of fracture healing in the tibia: mechanoregulation of cell activity using a lattice modeling approach. *Journal of orthopaedic research.* 2011;29(10):1496-1503.

21. Miramini S, Zhang L, Richardson M, Mendis P, Ebeling PR. Influence of fracture geometry on bone healing under locking plate fixations: A comparison between oblique and transverse tibial fractures. *Medical engineering & physics.* 2016;38(10):1100-1108.

22. Miramini S, Zhang L, Richardson M, et al. Computational simulation of the early stage of bone healing under different configurations of locking compression plates. *Computer methods in biomechanics and biomedical engineering.* 2015;18(8):900-913.

23. Lacroix D, Prendergast P. A mechano-regulation model for tissue differentiation during fracture healing: analysis of gap size and loading. *Journal of biomechanics.* 2002;35(9):1163-1171.

24. Isaksson H, Van Donkelaar CC, Huiskes R, Ito K. Corroboration of mechanoregulatory algorithms for tissue differentiation during fracture healing:

comparison with in vivo results. *Journal of Orthopaedic Research.* 2006;24(5):898-907.

25. Prendergast P, Huiskes R, Søballe K. Biophysical stimuli on cells during tissue differentiation at implant interfaces. *Journal of biomechanics.* 1997;30(6):539-548.

26. Zhang L, Miramini S, Mendis P, Richardson M, Pirpiris M, Oloyede K. The effects of flexible fixation on early stage bone fracture healing. *Int J Aerosp Lightweight Struct.* 2013;3(2):181-189.

27. Epari DR, Taylor WR, Heller MO, Duda GN. Mechanical conditions in the initial phase of bone healing. *Clinical Biomechanics.* 2006;21(6):646-655.

28. Klein P, Schell H, Streitparth F, et al. The initial phase of fracture healing is specifically sensitive to mechanical conditions. *Journal of orthopaedic research.* 2003;21(4):662-669.

29. Zhang L, Miramini S, Richardson M, et al. Computational modelling of bone fracture healing under partial weight-bearing exercise. *Medical Engineering & Physics.* 2017;42:65-72.

30. Duda GN, Mandruzzato F, Heller M, Kassi J-P, Khodadadyan C, Haas NP. Mechanical conditions in the internal stabilization of proximal tibial defects. *Clinical Biomechanics.* 2002;17(1):64-72.

31. GOM. ARAMIS user manual–Software. In: GOM mbH Braunschweig, Germany; 2013.

32. Gardiner B, Smith D, Pivonka P, Grodzinsky A, Frank E, Zhang L. Solute transport in cartilage undergoing cyclic deformation. *Computer methods in biomechanics and biomedical engineering.* 2007;10(4):265-278.

33. Carter DR, Beaupré GS, Giori NJ, Helms JA. Mechanobiology of skeletal regeneration. *Clinical orthopaedics and related research.* 1998;355:S41-S55.

34. Claes L, Heigele C. Magnitudes of local stress and strain along bony surfaces predict the course and type of fracture healing. *Journal of biomechanics.* 1999;32(3):255-266.
35. Perren S. Physical and biological aspects of fracture healing with special reference to internal fixation. *Clinical orthopaedics and related research.* 1979;138:175-196.
36. Isaksson H, Wilson W, van Donkelaar CC, Huiskes R, Ito K. Comparison of biophysical stimuli for mechano-regulation of tissue differentiation during fracture healing. *Journal of biomechanics.* 2006;39(8):1507-1516.
37. Huiskes R, Van Driel W, Prendergast P, Søballe K. A biomechanical regulatory model for periprosthetic fibrous-tissue differentiation. *Journal of materials science: Materials in medicine.* 1997;8(12):785-788.
38. Duda GN, Mandruzzato F, Heller M, et al. Mechanical boundary conditions of fracture healing: borderline indications in the treatment of unreamed tibial nailing. *Journal of Biomechanics.* 2001;34(5):639-650.
39. Lacroix D, Prendergast P. Three-dimensional simulation of fracture repair in the human tibia. *Computer Methods in Biomechanics & Biomedical Engineering.* 2002;5(5):369-376.
40. Nielsen JK, Saltzman CL, Brown TD. Determination of ankle external fixation stiffness by expedited interactive finite element analysis. *Journal of orthopaedic research.* 2005;23(6):1321-1328.
41. Zhang G. Geometric and material nonlinearity in tensioned wires of an external fixator. *Clinical Biomechanics.* 2004;19(5):513-518.
42. Zamani A, Oyadiji S. Analytical modelling of Kirschner wires in Ilizarov circular external fixator as pretensioned slender beams. *Journal of The Royal Society Interface.* 2009;6(32):243-256.

744 43. Zamani A, Oyadiji S. Theoretical and finite element modeling of fine Kirschner wires
745 in Ilizarov external fixator. *Journal of Medical Devices.* 2010;4(3):031001.
746 44. Einhorn TA. The cell and molecular biology of fracture healing. *Clinical*
747 *orthopaedics and related research.* 1998;355:S7-S21.
748 45. Claes L, Recknagel S, Ignatius A. Fracture healing under healthy and inflammatory
749 conditions. *Nature Reviews Rheumatology.* 2012;8(3):133.
750 46. Einhorn TA, Gerstenfeld LC. Fracture healing: mechanisms and interventions. *Nature*
751 *Reviews Rheumatology.* 2015;11(1):45.
752 47. Comiskey D, MacDonald B, McCartney W, Synnott K, O'Byrne J. The role of
753 interfragmentary strain on the rate of bone healing—a new interpretation and
754 mathematical model. *Journal of biomechanics.* 2010;43(14):2830-2834.
755 48. Claes L, Eckert-Hübner K, Augat P. The fracture gap size influences the local
756 vascularization and tissue differentiation in callus healing. *Langenbeck's archives of*
757 *surgery.* 2003;388(5):316-322.
758 49. Gessmann J, Jettkant B, Schildhauer TA, Seybold D. Mechanical stress on tensioned
759 wires at direct and indirect loading: a biomechanical study on the Ilizarov external
760 fixator. *Injury.* 2011;42(10):1107-1111.
761 50. Duda GN, Sollmann M, Sporrer S, et al. Interfragmentary motion in tibial osteotomies
762 stabilized with ring fixators. *Clinical orthopaedics and related research.*
763 2002;396:163-172.
764 51. Duda GN, Sporrer S, Sollmann M, et al. Interfragmentary movements in the early
765 phase of healing in distraction and correction osteotomies stabilized with ring fixators.
766 *Langenbeck's Archives of Surgery.* 2003;387(11-12):433-440.
767 52. Martini L, Fini M, Giavaresi G, Giardino R. Sheep model in orthopedic research: a
768 literature review. *Comparative medicine.* 2001;51(4):292-299.

53. Yamaji T, Ando K, Wolf S, Augat P, Claes L. The effect of micromovement on callus formation. *Journal of Orthopaedic Science.* 2001;6(6):571-575.

54. Augat P, Burger J, Schorlemmer S, Henke T, Peraus M, Claes L. Shear movement at the fracture site delays healing in a diaphyseal fracture model. *Journal of orthopaedic research.* 2003;21(6):1011-1017.

55. Claes LE, Heigele CA, Neidlinger-Wilke C, et al. Effects of mechanical factors on the fracture healing process. *Clinical orthopaedics and related research.* 1998;355:S132-S147.

56. Haines NM, Lack WD, Seymour RB, Bosse MJ. Defining the lower limit of a "critical bone defect" in open diaphyseal tibial fractures. *Journal of orthopaedic trauma.* 2016;30(5):e158-e163.

57. Fan Z, Swadener J, Rho J, Roy M, Pharr G. Anisotropic properties of human tibial cortical bone as measured by nanoindentation. *Journal of Orthopaedic Research.* 2002;20(4):806-810.

58. Rho J-Y. An ultrasonic method for measuring the elastic properties of human tibial cortical and cancellous bone. *Ultrasonics.* 1996;34(8):777-783.

59. McCartney W, Mac Donald B, Hashmi M. Comparative performance of a flexible fixation implant to a rigid implant in static and repetitive incremental loading. *Journal of materials processing technology.* 2005;169(3):476-484.

60. Davis JR. *Aluminum and aluminum alloys.* ASM international; 1993.

## Tables

**Table 1:** Properties of materials used in this study

| Material | E (MPa) | υ | Φ | k ($m^4 N^{-1} s^{-1}$) | $K_s$ (MPa) | $K_f$ (MPa) |
|---|---|---|---|---|---|---|
| Cortical bone | 20000 [23] | 0.3 [23] | 0.04 [23] | $10^{-17}$ [23] | 13920 [23] | 2300 [23] |
| Bone Marrow | 2 [23] | 0.167 [23] | 0.8 [23] | $10^{-14}$ [23] | 2300 [23] | 2300 [23] |
| Granulation Tissue | 0.05 [59] | 0.167 [23] | 0.8 [23] | $10^{-14}$ [23] | 2300 [23] | 2300 [23] |
| Stainless Steel | 197000 [14] | 0.29 [14] | -------- | -------- | -------- | -------- |
| Aluminium | 69000 [60] | 0.33 [60] | -------- | -------- | -------- | -------- |

**E** – Young's modulus **υ** - Poisson's Ratio **Φ** – Porosity **k** –Permeability

$\mathbf{K_s}$ – Solid compression modulus $\mathbf{K_f}$ – Fluid compression modulus

819

820

821 **Table 2:** Simulation cases used in this study

| Case | Control Case | Gap size (mm) | Ring diameter (mm) | Wire pre-tension (N) | Axial load (N) |
|---|---|---|---|---|---|
| ***1) Effect of gap size*** | | | | | |
| G1 | G3 | 1 | 155 | 883 (90 kg) | 150 |
| G3 | - | 3 | 155 | 883 (90 kg) | 150 |
| G5 | G3 | 5 | 155 | 883 (90 kg) | 150 |
| ***2) Effect of axial load*** | | | | | |
| F1a | G1 | 1 | 155 | 883 (90 kg) | 100 |
| F1b | G1 | 1 | 155 | 883 (90 kg) | 200 |
| F3a | G3 | 3 | 155 | 883 (90 kg) | 100 |
| F3b | G3 | 3 | 155 | 883 (90 kg) | 200 |
| F5a | G5 | 5 | 155 | 883 (90 kg) | 100 |
| F5b | G5 | 5 | 155 | 883 (90 kg) | 200 |
| ***3) Effect of ring diameter*** | | | | | |
| R1 | G1 | 1 | 130 | 883 (90 kg) | 150 |
| R3 | G3 | 3 | 130 | 883 (90 kg) | 150 |
| R5 | G5 | 5 | 130 | 883 (90 kg) | 150 |
| ***4) Effect of wire pre-tension*** | | | | | |
| P1a | G1 | 1 | 155 | 491 (50 kg) | 150 |
| P1b | G1 | 1 | 155 | 1275 (130 kg) | 150 |
| P3a | G3 | 3 | 155 | 491 (50 kg) | 150 |
| P3b | G3 | 3 | 155 | 1275 (130 kg) | 150 |

| | | | | | |
|---|---|---|---|---|---|
| P5a | G5 | 5 | 155 | 491 (50 kg) | 150 |
| P5b | G5 | 5 | 155 | 1275 (130 kg) | 150 |

**Bone fracture healing under Ilizarov fixator: influence of fixator configuration, fracture geometry and loading**

**Ganesharajah Ganadhiepan, Saeed Miramini, Minoo Patel, Priyan Mendis and Lihai Zhang***

**Brief abstract:** Using computational models validated by mechanical tests involving an advanced 3D optical measurement system, this study aims to enhance the understanding of the effect of Ilizarov fixator configuration, fracture geometry and external loading on bone fracture healing. The effects of fixator configuration and external loading on healing was found to be dependent on fracture gap size which was the most dominant parameter of all. The study exhibits the potential of computational models in assisting patient specific clinical treatment planning.

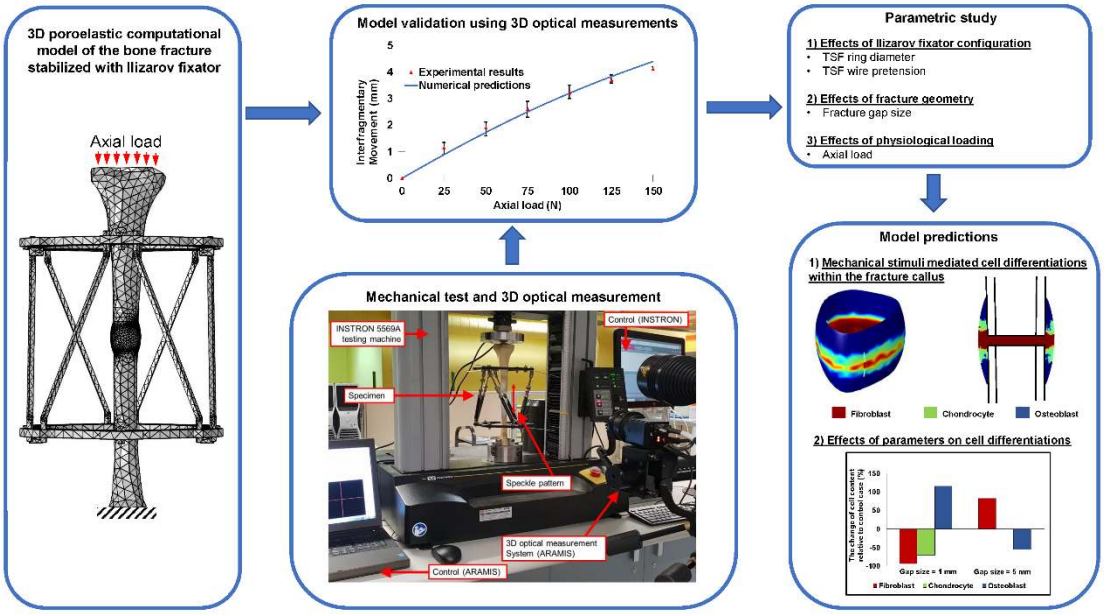

**Figure Captions**

**Figure 1** (a) Schematic diagram showing the configuration of the Taylor Spatial Frame (TSF) used in this study ; (b) The developed 3D finite element model of the fracture.

**Figure. 2** Methodology adopted in this study

**Figure 3** Details of experimental setup using INSTRON 5569A testing machine and 3D optical measurement system (ARAMIS).

**Figure 4** Comparison of axial interfragmentary movements (IFM) obtained from the experiment and numerical simulation of the experiment (gap size = 20 mm, wire pre-tension = 883 N (90 kg)) : (a)130 mm diameter ring and (b) 155 mm diameter ring.

**Figure 5** a) Computational model of the fractured tibia; b) schematic diagram of the longitudinal section of the fracture site showing different regions of the fracture site; and c) spatially dependent cell differentiations within the fracture callus, stabilized with Taylor spatial frame (ring diameter = 155 mm, wire pre-tension = 883 N (90 kg) and axial load = 150 N) under different gap sizes (i.e. 1 mm, 3 mm and 5 mm).

**Figure 6** The change of cell contents within different regions of the callus relative to control case G3 (ring diameter = 155 mm, gap size = 3 mm, wire pre-tension = 883 N (90 kg) and axial load = 150 N) under different gap sizes (i.e. 1 mm and 5 mm).

**Figure 7** The change of cell contents within different regions of the callus under different axial loads (i.e. 100 N and 200 N) relative to control case G1 for (a) 1 mm; relative to control case G3 for (b) 3 mm and relative to control case G5 for (c) 5 mm gap sizes (Note : Callus regions with negligible cell content changes are not shown).

**Figure 8** The change of cell contents within different regions of the callus under 130 mm diameter ring relative to control case G1 for (a) 1 mm; relative to control case G3 for (b) 3 mm and relative to control case G5 for (c) 5 mm gap sizes (Note : Callus regions with negligible cell content changes are not shown).

**Figure 9** The change of cell contents within different regions of the callus under different wire pretensions (i.e. 491 N (50 kg) and 1275 N (130 kg)) relative to control case G1 for (a) 1 mm; relative to control case G3 for (b) 3 mm and relative to control case G5 for (c) 5 mm gap sizes (Note : Callus regions with negligible cell content changes are not shown).

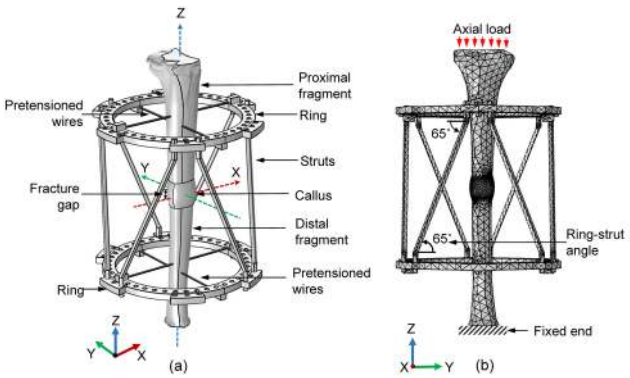


CNM_3199_F1_AA.tif

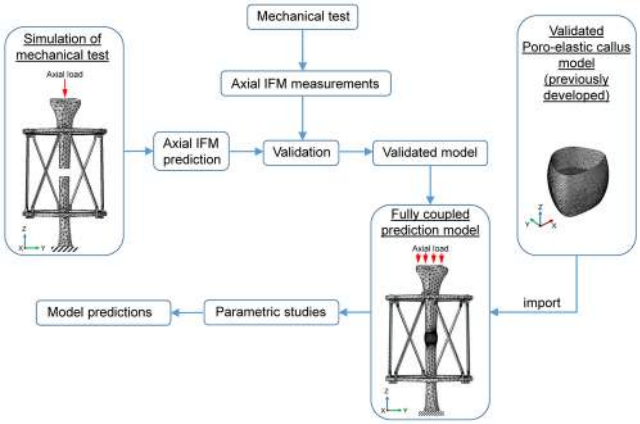


CNM_3199_F2_AA.tif

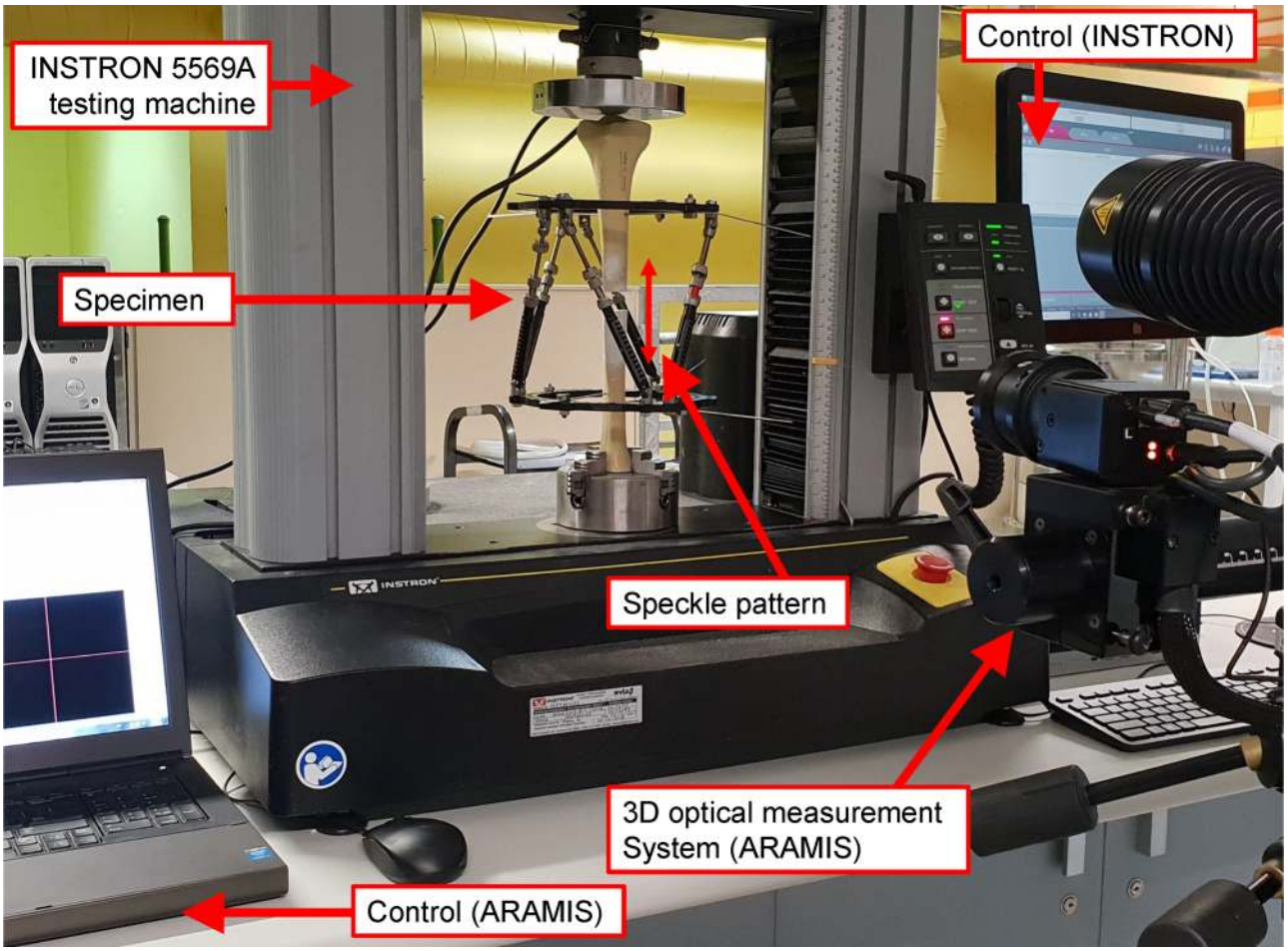


CNM_3199_F3_AA.tif

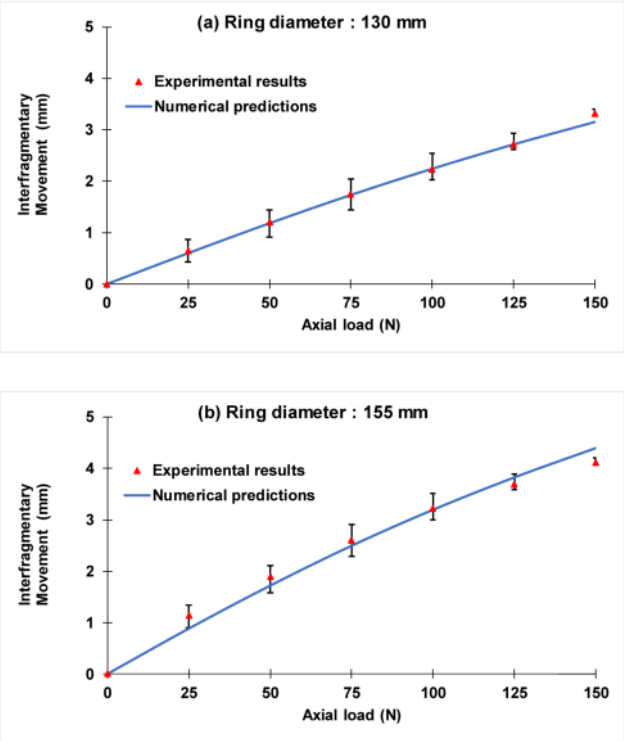


CNM_3199_F4_AA.tif

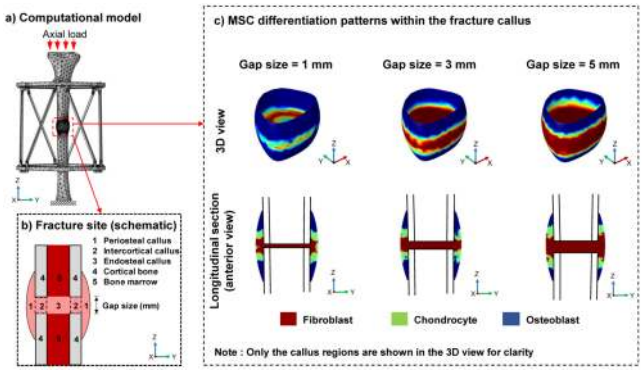


CNM_3199_F5_AA.tif

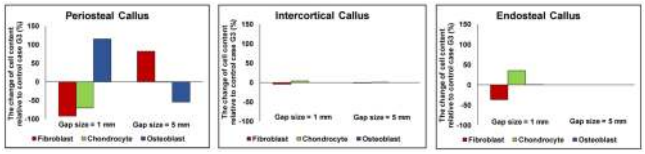


CNM_3199_F6_AA.tif

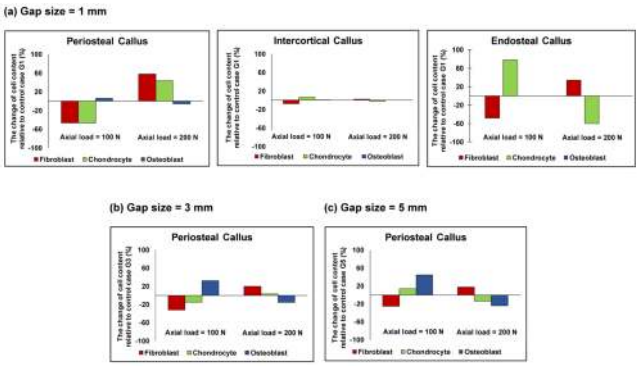


CNM_3199_F7_AA.tif

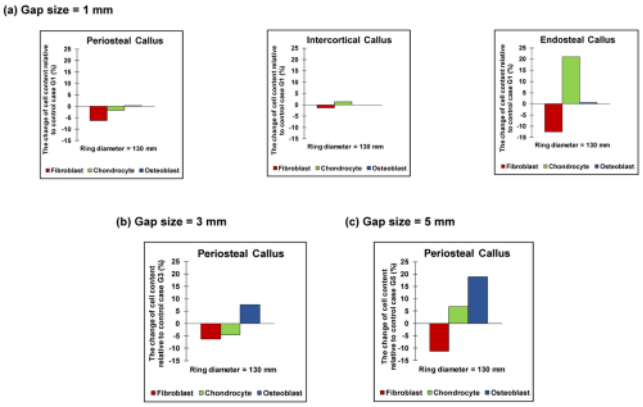


CNM_3199_F8_AA.tif

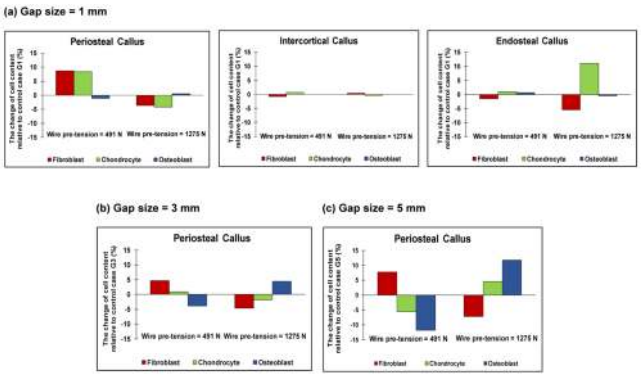


CNM_3199_F9_AA.tif

Author/s:
Ganadhiepan, G;Miramini, S;Patel, M;Mendis, P;Zhang, L

Title:
Bone fracture healing under Ilizarov fixator: Influence of fixator configuration, fracture geometry, and loading

Date:
2019-06-01

Citation:
Ganadhiepan, G., Miramini, S., Patel, M., Mendis, P. & Zhang, L. (2019). Bone fracture healing under Ilizarov fixator: Influence of fixator configuration, fracture geometry, and loading. INTERNATIONAL JOURNAL FOR NUMERICAL METHODS IN BIOMEDICAL ENGINEERING, 35 (6), https://doi.org/10.1002/cnm.3199.